KSME

Springer

Journal of Mechanical Science and Technology 36 (12) 2022

Original Article
DOI 10.1007/s12206-022-04 -y

Keywords:
· Radial loading
· Stress profile
· Cylindrical and spherical geometry
· Inflection point

Correspondence to:
Asghar Aryanfar
aryanfar@caltech.edu

Citation:
Aryanfar, A., Skafi, M. E., Goddard III, W. A. (2022). An estimation for the effective force transfer medium in radial loading of the cylindrical and spherical geometries. Journal of Mechanical Science and Technology 36 (12) (2022) ?~?. http://doi.org/10.1007/s12206-022-04 -y

Received ?? th, 2022
Revised ?? th, 2022
Accepted ?? th, 2022

† Recommended by Editor ??

An estimation for the effective force transfer medium in radial loading of the cylindrical and spherical geometries

Asghar Aryanfar[1,2], Mounir El Skafi[1] and William A. Goddard III[3]

[1]American University of Beirut, Riad El-Solh, Lebanon 1107 2020, [2]Bahçeşehir University, 4 Çırağan Cad, Beşiktaş, Istanbul, Turkey 34353, [3]California Institute of Technology, 1200 E California Blvd, Pasadena, CA 91125

Abstract The radial design of the cylindrical and spherical composites, subjected to the loading requires the quantitative understanding of their spatial stress distribution, which non-linearly depend on both geometry and the applied force. We develop a new framework for estimating the effective medium of the force transfer during considerable loads. Analyzing the horizontal stress profile, we have identified concave-to-convex behavior and we show that the bridging inflection point could be a measure for distinguishing the major force carrying region form the rest. Identifying such borderline, we have analytically estimated the effective force transfer medium, which has been validated via the simulation results and the respective curve-fitting into an oval. Finally, we have shown that having the same amount of material, the major force transfer region in $2D$ (cylinder) is ≈ 1.4 times larger than the $3D$ (sphere) case on the onset of yielding and $y_{EQ} \approx 0.53R$ as their equal stress elevation. The quantified force transfer region could help the design process of the radial composites subjected to considerable amount of force, with stronger surrounding, while the inner regions could compensate in strength.

1. Introduction

The analysis of the force and corresponding stress of the curved interfaces has been studied under the context of contact mechanics for several years [1-4], which was initiated from the first problem of the elastic deformation of parabolic surfaces by Heinrich Hertz [5, 6]. Throughout the years, other researchers have expanded on the mechanics of contact [7-11]. An extensive review of the literature on spherical and cylindrical contacts under normal load with and without friction, which anticipates the onset of yielding, was made by Adams and Nosonovsky [12]. In addition, Ghaednia et al. [10] have provided a comprehensive review of elastic-plastic contact mechanics.

Additionally, Chang et al. [13] have analyzed the onset of yielding of a spherical contact in the case of perfect slip using the stress field of Huber and the von Mises yield criterion. They calculated the critical interference at the inception of plastic deformation as a function of the mechanical properties and the radius of the sphere and Poisson's ratio. Later, Jackson and Green [14] introduced an empirical equation for the critical interface at the inception of yield, which is considerably different than the studies of Chang et al. [13, 15].

Kogut and Etsion [16] have numerically addressed the same mechanism for elasto-plastic contact under perfect slip condition while the composite disks have been addressed by Faisal et al. [17]. Etsion et al. [18] studied the process of loading-unloading of an elasto-plastic loaded sphere in contact with a rigid flat plate under perfect slip condition. They calculated the contact load, stresses, and deformations in the sphere during both loading and unloading for a wide range of interfaces and a variety of ductile material properties. The conditions required to initiate a brittle material failure of a spherical contact under perfect slip were studied by Fischer-Cripps [19, 2].

Goodman [20] addressed the first analytical solution for tangential stress distribution of the

non-slipping spherical contact while assuming Hertzian pressure distribution. Later, Spence [21] developed a more exact analysis by simultaneously solving the dual integral equations for shear and normal stress distributions, considering the total compressive load. He concluded that for smaller Poisson's ratio, the influence of shear stresses on the contact load is appreciable. Spence [22] extended his previous analysis for partial slipping using a finite friction coefficient. Kosior et al. [23] analyzed an elastic spherical contact under partial slip condition using a domain decomposition method coupled with boundary element method. They calculated the stress distribution, the contact radius, and the displacement as functions of the mechanical properties. Their results were in good agreement with the analytical solution of Spence [22].

Johnson et al. [24] extended the solution by Goodman [20] and found the radial stress distribution on the surface of the sphere both in the contact interface and inner regions. They solved the problem for the maximum tensile stress which causes fracture of brittle materials. Another extension of the Goodman's solution is by Hills and Sackfield [25] who gave a complete picture of the stress distribution assuming full and partial stick contact conditions. Recently, Zhupanska and Ulikto [26] used a similar approach to solve the contact of a rigid cylinder indenting an elastic half-space, both for non-slipping and slipping conditions with a finite friction coefficient. The oscillatory behavior of the sphere in the half-space has been analyzed by Kontomaris et al. [27], which has described an analytical solution in the range of $0.8R < r < 0.1R$, observing similarities with the normal spring contact with the elastic half-space.

Moreover, Du and Hu [28] have demonstrated a theoretical formulation of the compression behavior on knitted spacer fabrics with spherical geometries. Du and Hu [29] applied actual compression to the fabrics and compared the theoretical results in their previous paper to the experimental results which show agreement with the theoretical formulation with the maximum error of 18.2 %. Shi et al. [30] have explored the compression of convex shell and formulation where adhesion between the shell and the rigid plate occurs upon considerable deflection. This study can cover broad range from macroscopic to micro and nano scale applications. Ciavarella et al. [31] incorporated the adhesion role in the small-scale, which lead to instabilities in the load-displacement diagram in which approaching bodies jump in to contact, whereas separated bodies jump out at a tensile pull-off force. A more generic approach later has been proposed for the shear-induced contact of anisotropic bodies of any shape by Sahli et al. [32].

An important recent application of contact mechanics is in a broader application for computing the inter-particle forces of granular materials. Hurley et al. [33] have established a Granular Element Method (ETM) framework, where they utilized the experimental images using photo-elasticity for extracting these forces on opaque granular materials through experimental imaging. Later, Hurley et al. [34] validate their experimental approach with finite element analysis. They continued to experiment their method on stiff opaque 3D grains for both quartz crystals and ruby grains [35]. These inter-particle network forces are studied at the level of the grain; however, not much emphasis was done on the forces inside the grain per se. Additionally, Pejchal et al. [36] have studied the fracture of quartz crystals through the meridian crack test theory. They highlight that the highest stresses are at the top and bottom periphery of the spheres and that there are different trajectories for the peak tensile strength at the center and along the surface of the sphere. Particularly, they found that 5 % of the spheres failed below the strength ranging between 300-400 MPa due to the existence of internal pores.

Lin et al. [37] have conducted the studied the variable compression of the soft materials, where the experiments on rubber (i.e., incompressible) and sponge (i.e., compressible) showed close agreement with their respective developed model. They interpreted that incompressible material would exhibit higher lateral extension due to preserved material volume and that the compressible material will exhibit reduced porosity justifying the lower lateral extension.

In addition, an investigation on composite structures under lateral loading has been performed by Li et al. [38]. The study used Aluminum, glass fiber-reinforced polymer (GFRP) plastic, and carbon fiber-reinforced polymer (CFRP) plastic tubes with variable diameter to thickness ratio (i.e., d/t) to examine their strength upon lateral (i.e., radial) loadings through experiments and numerical simulations. It was found that the cost-effective Aluminum tubes have better crushing behavior compared to the composites which increases with the tube thickness, and it was related to its ductile response vs. brittle performance of GFRP and CFRP plastics. An interesting recent study was performed by was performed by Zhao et al. [39] where the compression of spherical shells due to multiple welded hollow spherical joints (WHSJ) has been investigated through random spotting of nodular corrosion through probabilistic modeling and anticipated the compressive strength under variation of geometrical parameters.

Numerical simulations have been widely performed on radial and spherical contact systems in various schemes. Faisal et al. [17] simulated and experimented diametral compression on cylinders to study the effect of surface coating on the surface and the internal shear stresses. The coating was found to be helpful in the coated zone in reducing the internal stresses of the disc. Similarly, Chen. et al. [40] have developed an analytical solution for the force-displacement behavior for the contact of dissimilar elastic spheres with coatings.

Han et al. [41] demonstrated the compression of iron nanospheres through numerical simulation by the aim of minimizing the size such that the failure is scale-independent. It was found out that the iron nano-spheres with a diameter less than 210 nm will have contact pressure saturated at 10.7 GPa where getting smaller does not increase the contact pressure value further. Chen et al. [42] have performed both experimental and numerical studies of sphere under compression and showed agreement in the obtained fracture pathways. An in-

teresting approach in using numerical simulation in contact mechanics is done by Vijaywargiya and Green [43] who used finite element modeling for bi-cylindrical contact, considering the sliding. This study highlights that in practice, perfectly vertical contact between curved surfaces is not tangible and that it is important to take sliding into consideration to better estimate the forces at the contact.

Although the above-mentioned studies highlight some aspects of the contact mechanics, none of them has established an effective framework for estimating the medium where the significant portion of the force is getting transferred, which is critical for layered design of the radial composites. Having the complexity and non-linear distribution of the stress which depends both on geometry as well as the applied load, in this paper, we establish a framework for estimating the effective force transfer medium ETM, which carries the significant portion of the radial load in the cylindrical and spherical geometries. Subsequently, we will obtain such medium, which resembles an oval, both via simulation with the finite element software and the mathematical regression and curve-fitting which resembles an oval. We have visualized estimated force transfer medium ETM, which resembles an oval, and visualized and verified it via matching of the three methods of analytical, simulation, and curve-fitting. The results could be utilized for the cost-effective design of the layered composite cylindrical and spherical geometries subjected to the radial loading, where we quantitatively could address the strength needed in the outer region, and relatively cost-effective material in the inner layers.

2. Methodology

The complexity of the contact mechanics gets higher when the component shape causes the simultaneous formation of the elastic and plastic stresses. In fact, radial geometries typically lead to higher variation in the area, such that the initial contact region is merely a point, which eventually turns into a finite surface after the infinitesimal deflection.

Regarding the optimization of the composition of the radial geometry, one needs to find the stress distribution. Therefore, the spherical ball could have a composition with varying mechanical properties (strength) in the radial direction as has been observed in our experimental sample in Fig. 1. Fig. 2 illustrates the schematics of such continuously layered composite subjected to the load *F*.

2.1 $F-\delta$ relationship:

The geometry of the corresponding deformation δ is detailed out in the Fig. 3, where the maximum vertical stress occurs in the boundary cross-section with the elevation y_0 and the real-time thickness of $w(\delta)\approx 2\sqrt{R\delta}$. The deformed outer boundary of the medium could be considered as multitudes of the infinitesimal bars deflected vertically to the magnitude of $\delta(x)$, stopping in the elevation $y := R-\delta/2$, where x is the

Fig. 1. Lab-made experimental sample illustrating the compositional heterogeneity

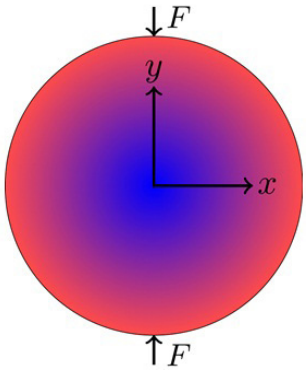

Fig. 2. Continuously layered radial composite.

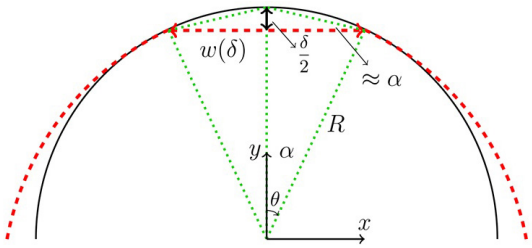

Fig. 3. Deformed shape (red, dashed) caused from the total infinitesimal displacement of δ.

measure in the lateral (i.e., horizontal) direction. Hence, the range of the interfacial angle θ would be:

$$-cos^{-1}\left(1-\frac{\delta}{2R}\right)<\theta<cos^{-1}\left(1-\frac{\delta}{2R}\right)$$

Therefore, neglecting the minimum strain in the ends[1], the respective strain in each infinitesimal bar $\epsilon(\theta)$ is obtained as:

$$\epsilon(\theta)=1-\frac{1}{\cos\theta}\left(1-\frac{\delta}{2R}\right)$$

[1] The minimum strain ϵ_{min} is associated with the settling down the entire interface upon loading.

where θ is the respective angle from the vertical direction. From the geometry $x = R\sin\theta$ one has: $dx = R\cos\theta d\theta$, and the total applied force in two-dimensional loading F_{2D} could get integrated as:

where b is the in-plane thickness of the cylinder. Eq. (1) in fact shows a non-linear relationship between the force F and the deflection δ. Regarding the three-dimensional case, we consider an equivalent shape which carries same amount of the materials (volume) such that $V_{3D} \coloneqq V_{2D}$. Hence, the cylindrical thickness b and the spherical radius R is obtained as:

$$b = \frac{4}{3}R$$

and one can obtain the three-dimensional force on the sphere F_{3D} as:

$$F_{3D} = \int_0^{\frac{l}{2}} \left(E\left(1 - \frac{1}{\cos\theta}\left(1 - \frac{\delta}{2R}\right)\right)\right) 2\pi x dx = \cdots = \frac{\pi E}{4}\delta^2$$

which estimates the quadratic relationship between the force F and the displacement δ. For both cases, in the elastic deformation the maximum stress $\sigma_{max}(y_0)$ occurs in the center, and assuming the deflection of an infinitesimal bar, we have:

$$\sigma_{\max}(y_0) = E\frac{\delta}{2R}$$

2.2 Effective force transfer medium ETM

The vertical variations in the stress profile are schematically presented in the Fig. 4, where moving deeper makes the stress profile getting flattened out. Two trends are discernible as below:

1) The stress value peaks directly under the force point and drops sharply moving laterally away from it in the x-direction. This forms a convex (curved outward) stress profile in the central zone, which is the most obvious in the upper boundary (i.e. red).

2) Moving lower into the depth ($y-$direction) makes the cross section larger-spanned in the $x-$direction, which is far-enough from the force. Therefore, the stress value will diminish in magnitude and variation, forming a concave (curved inward) profile that converges to the minimal value[2].

Such convex-to-concave change in the stress profile, which is connected via an inflection point is illustrated and characterized in the Fig. 5. Considering the areas before and after the inflection point, we have:

[2] We consider the minimum stress negligible here, although not affecting the framework.

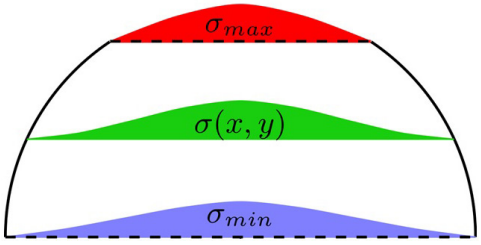

Fig. 4. Schematics of the stress profile in depth.

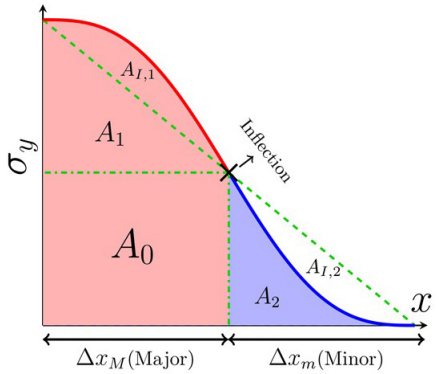

Fig. 5. The half-stress profile (due to symmetry) with the major (red) and minor (blue) force carrying regions, separated by the inflection point.

$$A_0 + A_1 + A_{I,1} \gg A_2 + A_{I,2}$$

which means that most of the force is carried before the inflection point and the remaining residue is insignificant. This is particularly true when the inflection point is half-way from the center (i.e., $\Delta x_M \approx \Delta x_m$), where the simplifying leads to:

$$\frac{\sigma_y}{2} \times \Delta x_M + A_{I,1} + A_{I,2} \gg 0$$

which proves that the central region, before the inflection point (Δx_M) bears a significant part of the load, while the peripheral zone (Δx_m) remain to carry relatively negligible stress [44].

For analytical estimation for the ETM in two dimensions (i.e., cylinder), we assume that the border zone has the form of $x_{2D} = f(y)$. Since moving vertically from the top boundary toward the center widens the cross-sectional area with the half width of $\sqrt{R^2 - y^2}$ and flattens the stress distribution, one expects that the major force carrying medium widens as well. On the other hand, since applying larger force F makes wider footprint of thickness $w(\delta)$ in the boundary, the involved volume for

the force transfer should get enlarge as well. Identifying these two major factors, here-in we estimate the border-zone of the ETM to be the average of the aforementioned factors as visualized in the Fig. 6:

$$x_{2D} \approx \frac{1}{2}\left(\sqrt{R\delta} + \sqrt{R^2 - y^2}\right) \quad (2)$$

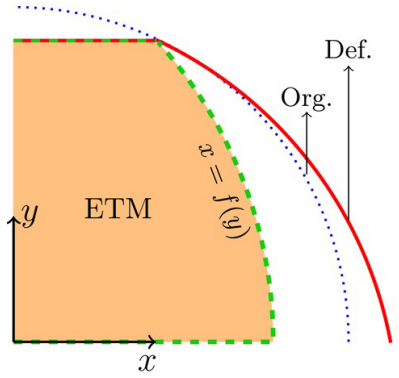

Fig. 6. Effective transfer medium (ETM), with the original (Org.) and deformed (Def.) shapes.

An obvious point of interest for the effective force transfer medium is in the top margin, where the deflected outer and ETM boundaries coincide. In both $2D$ and $3D$ cases, the location of the border-zone for the ETM is obtained as both function of geometry (i.e., R) and the applied force F, which translates into the deflection δ.

Regarding the $3D$ case the in-plane depth additionally has an extra effect since the footprint of the force is a circle rather than a rectangle. Such additional effect of the deflection δ could get counted-in the weighted sum, making the border zone for ETM as:

$$x_{3D} \approx \frac{2}{3}\sqrt{R\delta} + \frac{1}{3}\sqrt{R^2 - y^2} \tag{3}$$

2.3 Simulation

The simulation has been carried out in the ABAQUS software using the variables given in the Table 1 for the cylindrical ($2D$) and spherical ($3D$) geometries. For the elastic simulation, the imposed radial deflection makes sure that the maximum Von-Mises stress does not exceed the ultimate strength σ_{ut}, and thus, no failure occurs. Fig. 7 shows the resulted Von-Mises stress distribution over a cross section of the cylinder before (left) and after (right) the failure. While the former figure shows the realistic distribution of the stress, the latter better illustrates the effective transfer medium ETM by the colored stress range visually.

As well, the Fig. 8 shows the similar resulted stress distribution for the spherical geometry before (left) and after (right) reaching the failure. Since the effective area in the sphere varies with higher rate than the cylindrical geometry by elevation, the required displacement before the yielding is lower not to yield to the failure. Due to such high stress variation in the stress, the color representation in $3D$ has been shown in log scale.

The horizontal profile for the Von-mises stress distribution $\sigma(x)$ are exported by defining a path from the center horizontally up to the boundary. Subsequently, the locus of the inflection points is plotted at several elevations in the Fig. 9.

Table 1. Simulation parameters.

Parameter	Value	Unit	Ref.
E	200	GPa	[45]
ν	0.32	[ ]	[46]
σ_y	250	MPa	[47]
σ_{ut}	365	MPa	[48]
R	0.2	m	Assumed
b	0.266	m	Assumed
# Meshes	$\sim 10^4$	[ ]	Assumed
ρ	7900	$kg.m^{-3}$	Assumed[3]
$\delta_{2D,El}$	0.6	mm	Assumed
$\delta_{3D,El}$	0.22	mm	Assumed
$\delta_{2D,Hyp}$	20	mm	Assumed
$\delta_{3D,Hyp}$	6	mm	Assumed

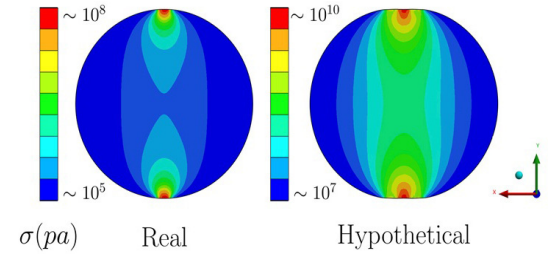

Fig. 7. 2D stress map during the linear behavior (left) and after yielding (right).

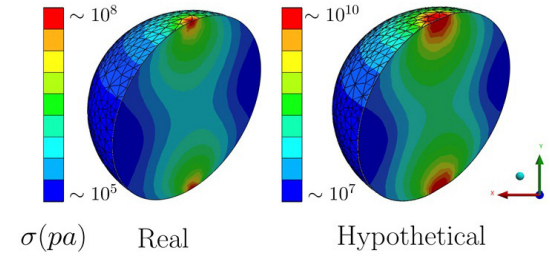

Fig. 8. 3D stress map during the linear behavior (left) and after yielding (right).

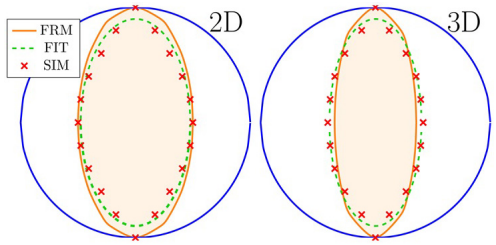

Fig. 9. Verification of effective transfer medium ETM (FRM: formula, FIT: curve fitting, SIM: simulation).

[3] https://www.geocentrix.co.uk/help/content/items/steels/structural_steels.htm

3. Results and discussion

The stress profile schematized in the Fig. 5 and presented in the Fig. 4 possesses the convex-to-concave behavior that could be addressed via curve-fitting into a logistic S-curve. Analogous to the horizontal stress profile, such curve is an intuitive method to predict dynamical behavior in the systems that begin and end with a finite value with the connecting inflection point. Therefore, the $S-$curve can be utilized for locating the border-zone of the effective force transfer medium ETM, which is expressed analytically in the form of [49, 50]:

$$\sigma(x)=\frac{a}{1+\exp\left(-b\left(x+c\right)\right)}+d$$

where *a, b, c, d* are constants obtained by curve-fitting. Afterwards, the inflection points x_c is directly obtained by locating the zero-curvature point as:

$$\frac{\partial^2\sigma}{\partial x^2}\approx 0\rightarrow x_c=-c$$

Consequently, the zone of the effective transfer medium ETM is obtained by connecting he extracted inflection points in various elevations, which finally resembles the shape of an oval. Assuming the form of $x^2/a^2+y^2/b^2=1$, the respective elliptic parameters $\{a,b\}\in\mathbb{R}$ are attained by means of minimizing the difference error, as shown below:

$$\text{Minimize } Err=\left|\sum_{k=1}^{n}\left(\frac{x_k^2}{a_i^2}+\frac{y_k^2}{b_i^2}-1\right)\right|$$

The attained regions for the effective force transfer medium ETM from either the formulation (Eqs. (2) and (3)), simulation or curve fitting are presented in the Fig. 9, which is in visual agreement with each other. In fact, the obtained zone resembles the attained *onion peel* convergent cone crack in spherical loading, which shows the critical fracture pathway [42]. Furthermore, the effective force transfer medium ETM toward the center has a wider area, which leads to less stress values and hence a softer layer could be used in that zone.

It is observed that effective force transfer medium ETM is thinner in $3D$ than in $2D$. The underlying reason is that the area of the sphere is proportional to $\sim R^2-y^2$ while for the cylinder it is $\sim\sqrt{R^2-y^2}$, therefore, the sensitivity of the $3D$ to the elevation change (y) is higher. In the boundary regions, the sphere has smaller cross-section $(A_{2D}=\frac{8}{3}R^{3/2}\delta^{1/2}\gg A_{3D}=\pi R\delta)$ since $\delta\ll R$, leading to the larger stress values, therefore the assigned deflection value for $3D$ is less, which generates a thinner ETM (Eq. (3)). However, moving toward the center, the spherical cross-sectional area increases with faster pace, ending up in larger value in the center $(\pi R^2$ for sphere $>\frac{8}{3}R^2$ in the volume-equal cylinder). Therefore, there is a crossing point y_{EQ}, where the $2D$ and $3D$ stress values are equal (i.e., $\sigma_{2D}=\sigma_{3D}$) assuming uniform stress, given the same deflection δ. Hence, we get:

$$y_{EQ}\approx 0.53R$$

which means that, having the same amount of material for the zones of $y>y_{EQ}$ the $3D$ average stress will be higher than $2D$ version $(\sigma_{3D}>\sigma_{2D})$ and vice-versa.

It is evident from the estimations of the ETM in Eqs. (2) and (3) that its area in the spherical ($3D$) geometry is smaller than that of the cylinder ($2D$) of equivalent material, which explains that the applied force on the sphere is less spread laterally, generating higher stress values relative to the cylinder. For the cylinder, the area of the ETM is:

$$A_{2D,ETM}=4\int_0^R x_{2D}dy$$
$$\ldots=2R\sqrt{R\delta}+\frac{\pi R^2}{2}$$

and the total area of a cylinder is:

$$A_{2D}=\pi R^2$$

Therefore, the effective ratio $\frac{A_{2D,ETM}}{A_{2D}}$ resembles the significant force-carrying portion of the medium. Noting $\epsilon=\frac{\delta}{2R}$ it is obtained as:

$$\frac{A_{2D,ETM}}{A_{2D}}=\frac{1}{2}+\frac{2\sqrt{2\epsilon}}{\pi}$$

In addition, the maximum strain in the most ideal case is 0.2 % for an elastic behavior (before yielding) [51], which leads to $\left(\frac{A_{2D,ETM}}{A_{2D}}\right)_{max}\approx 0.54$. This means that only 54 % of the whole cross-sectional area carries the significant amount of the applied force. Similarly, for the sphere, the area of the ETM would be:

$$A_{3D,ETM}=4\int_0^R x_{3D}dy$$
$$\ldots=\frac{8}{3}R\sqrt{R\delta}+\frac{\pi R^2}{3}$$

whereas the total area A_{3D} is identical to 2D. Hence, the effective areal ratio in spherical geometry is attained as:

$$\frac{A_{3D,ETM}}{A_{3D}}=\frac{1}{3}+\frac{8\sqrt{2\epsilon}}{3\pi}$$

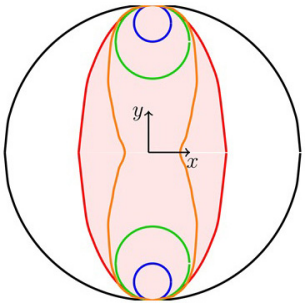

Fig. 10. Transition from the circular stress concentration region to the oval shape, by gradual increase in the force F.

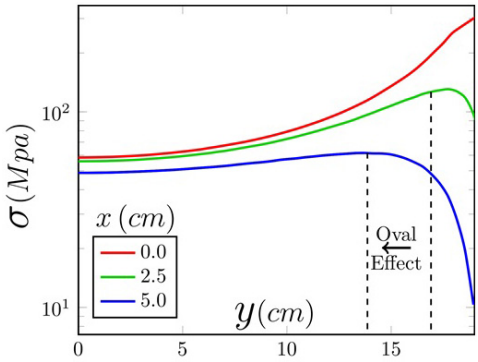

Fig. 11. ETM Oval-shape verification for *large-enough* applied force.

Likewise, considering 0.2 % yield criterion we get $\left(\frac{A_{3D,ETM}}{A_{3D}}\right)_{max}$ $\approx$ 0.39, which means that only 39 % of the area is effectively carrying the substantial amount of the imposed force. Therefore, the ETM in 2D is ~1.4 times larger than 3D. This explains that the forces are more distributed in the cylinder, and thus, more displacement is allowed before yielding ($\delta_{2D} > \delta_{3D}$).

Finally, the effective force transfer medium ETM has been approximated by solely the horizontal variation of the stress profile (*x*-direction). However, the vertical variation in the critical zone, would highly depend on the relative magnitude of the applied force *F*. The gradual increase in the force causes the critical zone to grow, as illustrated in the Fig. 10, which starts from the circular shape at the top and bottom as the stress-concentration regions and transitions into an oval shape as they grow and join each other. The existence of such preliminary circular zones can get interpreted from the force-deflection studies on the shells, which contain their material in the boundary and therefore, resist the highest during the initial stages of the loading [38].

In fact, the estimation for the effective force transfer medium ETM considers the case of considerable loadings (i.e., red), whereas for the lower load magnitudes, the stress in the central regions remains insignificant. For large enough applied force F, if one tracks the stress values vertically (along y direction) in different horizontal distances, there will be increasing trend reaching to the maximum limit, and at a certain elevation, the stress value suddenly gets a steep drop, as shown in the Fig. 11. While the former is due to decrease in total area (and therefore increasing the stress value), the latter occurs when the point exceeds the critical zone represented by ETM, since the oval shape of ETM narrows-down toward the top of the circular geometry. Additionally, this justifies the no-drop in stress at the center-line x = 0 since the entire path falls inside the ETM. In fact, reaching the maximum value is another proof for the existence of an effective force transfer medium ETM with oval shape that carries the highest portion of the applied force.

4. Conclusions

In this paper, we have developed a new framework for estimating the effective force transfer medium ETM during the radial loading of the 2D (cylindrical) and 3D (spherical) geometries. Analyzing the profile of stress distribution from the center to the periphery, we have identified curvature-changing behavior, where we have shown that the corresponding inflection point distinguishes the major and minor force-bearing regions. Subsequently, we have estimated such critical zone analytically versus the imposed load (and the resulted deflection) as well as the boundary of the medium. We have attained that the identified effective force transfer medium ETM carries the major portion of the imposed compressive force, where the rest of the medium remains insignificant.

Performing simulations, we have additionally shown that for large-enough applied force, which is beyond making solely stress-concentration zones, the ETM resembles and oval, which has been characterized via curve-fitting of the inflection locus. Furthermore, we have shown a very close agreement between the analytical and the simulation estimation for the effective force transfer medium ETM which has previously been interpreted as the possible fracture pathway. Analyzing the equivalent 2D and 3D geometries, we have shown that the 3D ETM is $\approx$ 1.4 times smaller than the 2D version of the same volume, opening the room for more deflection in the 2D case. Moving from center to the boundary, the cross-sectional area in the 3D zone starts with larger and ends with smaller value, relative to 2D, leaving the equal stress elevation of $y_{EQ} \approx 0.53R$. Current efforts on the next steps are in track for analytical calculation of the force deflection behavior of the core-shell radial composites consisting of multiple layers and their equivalent stiffness. The results are useful for the design of multilayered radial structures undergoing considerable loads, since they quantify the utilization of materials with a relatively lower strength toward the center, while using stronger layers on their surroundings.

Nomenclature

σ_y	: Yield stress (*pa*)
σ_{ut}	: Ultimate strength (*pa*)
R	: Radius of circular geometry (*m*)

b : Thickness of cylinder (m)
E : Elastic modulus (pa)
v : Poisson's ratio ([])
ρ : Density ($kg \cdot m^{-3}$)
F_{2D} : 2-dimensional force on a cylinder (N)
F_{3D} : 3-dimensional force on a sphere (N)
δ : Total deflection (m)
$\delta_{2D,El}$: Elastic deflection of the cylinder (m)
$\delta_{3D,El}$: Elastic deflection of the sphere (m)
$\delta_{2D,Hyp}$: Hypothetical deflection of the cylinder (m)
$\delta_{3D,Hyp}$: Hypothetical deflection of the sphere (m)

Acknowledgment

The authors would like to thank the support from Masri Institute at American University of Beirut, Grant Award No. 103919 for the student Mounir El Skafi.

Data availability

The raw data for producing the results in this manuscript are freely available upon request from the corresponding author at aryanfar@caltech.edu.

Conflict of interest statement

The authors declare that they have no competing financial interests to influence the work reported in this paper.

References

[1] K. L. Johnson, Contact mechanics cambridge univ. Press, Cambridge, 95 (1985) 365.
[2] A. C. Fischer-Cripps, Introduction to contact mechanics, *Springer* (2007).
[3] J. R. Barber and M. Ciavarella, Contact mechanics, *International Journal of Solids and Structures*, 37 (1-2) (2000) 29-43.
[4] K. L. Johnson, K. Kendall and aAD Roberts, Surface energy and the contact of elastic solids, Proceedings of the royal society of London. A. mathematical and physical sciences, 324 (1558) (1971) 301-313.
[5] K. L. Johnson, One hundred years of hertz contact, *Proceedings of the Institution of Mechanical Engineers*, 196 (1) (1982) 363-378.
[6] K. Knothe, History of wheel/rail contact mechanics: from redtenbacher to kalker, *Vehicle System Dynamics*, 46 (1-2) (2008) 9-26.
[7] J. A. Greenwood and J. B. Pl Williamson, Contact of nominally flat surfaces, Proceedings of the royal society of London, Series A. Mathematical and physical sciences, 295 (1442) (1966) 300-319.
[8] J. F. Archard. Elastic deformation and the laws of friction, *Proceedings of the Royal Society of London, Series A. Mathematical and Physical Sciences*, 243 (1233) (1957) 190-205.
[9] D. Tabor, The hardness of metals, Oxford university press (2000).
[10] H. Ghaednia, X. Wang, S. Saha, Y. Xu, A. Sharma and R. L. Jackson, A review of elastic-plastic contact mechanics, *Applied Mechanics Reviews*, 69 (6) (2017).
[11] R. L. Jackson, H. Ghaednia, H. Lee, A. Rostami and X. Wang, Contact mechanics, Tribology for scientists and engineers, pages (2013) 93-140.
[12] G. G. Adams and M. Nosonovsky, Contact modeling forces, Tribology international, 33 (5-6) (2000) 431-442.
[13] W.-R. Chang, Contact, adhesion, and static friction of metallic rough surfaces, *Ph.D. Thesis*, University of California, Berkeley (1986).
[14] R. L. Jackson and I. Green, A finite element study of elasto-plastic hemispherical contact against a rigid flat, *J. Trib.*, 127 (2) (2005) 343-354.
[15] W.-R. Chang, I. Etsion and D. B. Bogy, Static friction coefficient model for metallic rough surfaces (1988).
[16] L. Kogut and I. Etsion, Elastic-plastic contact analysis of a sphere and a rigid flat, *J. Appl. Mech.*, 69 (5) (2002) 657-662.
[17] N. H. Faisal, L. Mann, C. Duncan, E. Dunbar, M. Clayton, M. Frost, J. McConnachie, A. Fardan and R. Ahmed, Diametral compression test method to analyse relative surface stresses in thermally sprayed coated and uncoated circular disc specimens, *Surface and Coatings Technology*, 357 (2019) 497- 514, 2019.
[18] I. Etsion, Y. Kligerman and Y. Kadin, Unloading of an elastic–plastic loaded spherical contact, *International Journal of Solids and Structures*, 42 (13) (2005) 3716-3729.
[19] A. C. Fischer-Cripps, Predicting hertzian fracture, *Journal of Materials Science*, 32 (5) (1977) 1277-1285.
[20] L. E. Goodman, Contact stress analysis of normally loaded rough spheres (1962).
[21] DA2269050172 Spence. Self similar solutions to adhesive contact problems with incremental loading, *Proceedings of the Royal Society of London. Series A. Mathematical and Physical Sciences*, 305 (1480) (1968) 55-80.
[22] D. A. Spence, The hertz contact problem with finite friction. *Journal of Elasticity*, 5 (3-4) (1975) 297-319.
[23] F. Kosior, N. Guyot and G. Maurice, Analysis of frictional contact problem using boundary element method and domain decomposition method, *International Journal for Numerical Methods in Engineering*, 46 (1) (1999) 65-82.
[24] K. L. Johnson, J. J. O'connor and A. C. Woodward, The effect of the indenter elasticity on the hertzian fracture of brittle materials, *Proceedings of the Royal Society of London. A. Mathematical and Physical Sciences*, 334 (1596) (1973) 95-117.
[25] D. A. Hills and A. Sackfield, The stress field induced by normal contact between dissimilar spheres (1987).
[26] O. I. Zhupanska and A. F. Ulitko, Contact with friction of a rigid cylinder with an elastic half-space, *Journal of the Mechanics and Physics of Solids*, 53 (5) (2005) 975-999.
[27] S.-V. Kontomaris and A. Malamou, Small oscillations of a rigid sphere on an elastic half space: a theoretical analysis, *European Journal of Physics*, 41 (5) (2020) 055004.
[28] Z. Du and H. Hu, A study of spherical compression properties

of knitted spacer fabrics part I: theoretical analysis, *Textile Research Journal*, 82 (15) (2012) 1569-1578.
[29] Z. Du and H. Hu, A study of spherical compression properties of knitted spacer fabrics part II: comparison with experiments, *Textile Research Journal*, 83 (8) (2013) 794-799.
[30] J. Shi, S. Müftü and K.-T. Wan, Adhesion of an elastic convex shell onto a rigid plate, *The Journal of Adhesion*, 87 (6) (2011) 579-594.
[31] M. Ciavarella, J. Joe, A. Papangelo and J. R. Barber, The role of adhesion in contact mechanics, *Journal of the Royal Society Interface*, 16 (151) (2019) 20180738.
[32] R. Sahli, G. Pallares, A. Papangelo, M. Ciavarella, C. Ducottet, N. Ponthus and J. Scheibert, Shear- induced anisotropy in rough elastomer contact, *Physical Review Letters*, 122 (21) (2019) 214301.
[33] R. Hurley, E. Marteau, G. Ravichandran and J. E. Andrade, Extracting inter- particle forces in opaque granular materials: beyond photoelasticity, *Journal of the Mechanics and Physics of Solids*, 63 (2014) 154-166.
[34] R. C. Hurley, K. W. Lim, G. Ravichandran and J. E. Andrade, Dynamic inter-particle force inference in granular materials: method and application, *Experimental Mechanics*, 56 (2) (2016) 217-229.
[35] R. C. Hurley, S. A. Hall, J. E. Andrade and J. Wright, Force measurements in stiff, 3d, opaque granular materials, *In EPJ Web of Conferences*, 140 (2017) 02006, EDP Sciences.
[36] V. Pejchal, G. Žagar, R. Charvet, C. Dénéréaz and A. Mortensen, Compression testing spherical particles for strength: theory of the meridian crack test and implementation for microscopic fused quartz, *Journal of the Mechanics and Physics of Solids*, 99 (2017) 70-92.
[37] Y.-L. Lin, D.-M. Wang, W.-M. Lu, Y.-S. Lin and K.-L. Tung, Compression and deformation of soft spherical particles, *Chemical Engineering Science*, 63 (1) (2008) 195-203.
[38] S. Li, X. Guo, Q. Li, D. Ruan and G. Sun, On lateral compression of circular aluminum, cfrp and gfrp tubes, *Composite Structures*, 232 (2020) 111534.
[39] Z. Zhao, H. Liu and B. Liang, Probability distribution of the compression capacity of welded hollow spherical joints with randomly located corrosion, *Thin-Walled Structures*, 137 (2019) 167-176.
[40] X. W. Chen and Z. Q. Yue, Contact mechanics of two elastic spheres reinforced by functionally graded materials (fgm) thin coatings, *Engineering Analysis with Boundary Elements*, 109 (2019) 57-69.
[41] W.-Z. Han et al., From smaller is stronger to size- independent strength plateau: towards measuring the ideal strength of iron, *Advanced Materials*, 27 (22) (2015) 3385-3390.
[42] T. Chen, Q. Fang, Z. Wang and W. Zhu, Numerical simulation of compression breakage of spherical particle, *Chemical Engineering Science*, 173 (2017) 443-454.
[43] R. Vijaywargiya and I. Green, A finite element study of the deformations, forces, stress formations, and energy losses in sliding cylindrical contacts, *International Journal of Non- Linear Mechanics*, 42 (7) (2007) 914-927.
[44] A. R. Savkoor and G. A. D. Briggs, The effect of tangential force on the contact of elastic solids in adhesion, *Proceedings of the Royal Society of London. A. Mathematical and Physical Sciences*, 356 (1684) (1977) 103-114.
[45] J. Čapek, M. Machová, M. Fousová, J. Kubásek, D. Vojtěch, J. Fojt, E. Jablonska, J. Lipov and T. Ruml, Highly porous, low elastic modulus 316l stainless steel scaffold prepared by selective laser melting, *Materials Science and Engineering: C*, 69 (2016) 631-639.
[46] H. M. Ledbetter, Stainless-steel elastic constants at low temperatures, *Journal of Applied Physics*, 52 (3) (1981) 1587-1589.
[47] N. N. Samie, Disciplines involved in offshore platform design, *Practical Engineering Management of Offshore Oil and Gas Platforms* (2016) 25-212.
[48] J. E. Shigley, Shigley's mechanical engineering design, *Tata McGraw-Hill Education* (2011).
[49] T. Modis, Strengths and weaknesses of s-curves, *Technological Forecasting and Social Change*, 74 (6) (2007) 866-872.
[50] D. Kucharavy and R. D. Guio, Application of s-shaped curves, *Procedia Engineering*, 9 (2011) 559-572.
[51] R. A. Flinn and P. K. Trojan, Engineering materials and their applications, *Houghton Mifflin* (1975).

Asghar Aryanfar, is Assistant Professor of Mechanical Engineering at American University of Beirut. He received Ph.D. from California Institute of Technology, Pasadena, CA in 2015 and his research is on the multiphysical modeling of nonlinear events in heterogenous media.

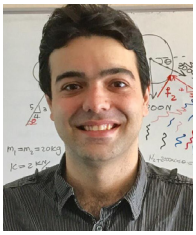

Mounir El Skafi, is Research Assistant in Department of Mechanical Engineering at American University of Beirut. His research interests are on Solid Mechanics and Materials Science.

William A. Goddard III is Charles and Mary Ferkel Professor of Applied Physics and Materials Science at California Institute of Technology. His research lies on the chemistry of materials and energy systems.